Lowest electronic states of neutral and ionic LiN

Mohammadi, Mohsen Doust; Bhaskaran, Renjith; Abdullah, Hewa Y.; Abdallah, Hassan H.; Biskos, George; Bhowmick, Somnath

DOI
10.1002/qua.27288

Publication date
2023

Document Version
Final published version

Published in
International Journal of Quantum Chemistry

Received: 14 July 2023 | Revised: 27 October 2023 | Accepted: 30 October 2023

DOI: 10.1002/qua.27288

RESEARCH ARTICLE

International Journal of Quantum Chemistry WILEY

Lowest electronic states of neutral and ionic LiN

Mohsen Doust Mohammadi[1] | Renjith Bhaskaran[2] | Hewa Y. Abdullah[3] | Hassan H. Abdallah[4] | George Biskos[1,5] | Somnath Bhowmick[1]

[1]Climate and Atmosphere Research Centre, The Cyprus Institute, Nicosia, Cyprus

[2]Department of Chemistry, Madanapalle Institute of Technology & Science, Madanapalle, Andhra Pradesh, India

[3]Physics Education Department, Faculty of Education, Tishk International University, Erbil, Iraq

[4]Chemistry Department, College of Education, Salahaddin University-Erbil, Erbil, Iraq

[5]Faculty of Civil Engineering and Geosciences, Delft University of Technology, Delft, CN, The Netherlands

Correspondence
Somnath Bhowmick, Climate and Atmosphere Research Centre, The Cyprus Institute, Nicosia 2121, Cyprus.
Email: s.bhowmick@cyi.ac.cy

Funding information
Republic of Cyprus through the Research and Innovation Foundation project ML-NANOCAT, Grant/Award Number: CODEVELOP-GT/0322/0093; European Union's Horizon 2020 Research and Innovation Program, Grant/Award Number: 856612; Government of the Republic of Cyprus

Abstract

We have investigated the potential energy curves (PECs) of the LiN heteronuclear diatomic molecule, including its ionic species LiN^+ and LiN^-, using explicitly correlated multi-reference configuration interaction (MRCI-F12) calculations in conjunction with the correlation consistent quintuple-ζ basis set. The effect of core–valence correlation, scalar relativistic effects, and the size of the basis sets has been investigated. A comprehensive set of spectroscopic constants determined based on the above-mentioned calculations are also reported for the lowest electronic states and all systems, including dissociation energies, harmonic and anharmonic vibrational frequencies, and rotational constants. Additional parameters, such as the dipole moments, equilibrium spin-orbit constants, excitation energies, and rovibrational energy levels, are also documented. We found that the three triplet states of LiN, namely, X $^3\Sigma^-$, A $^3\Pi$, and 2 $^3\Sigma^-$, exhibit substantial potential wells in the PEC diagrams, while the quintet states are repulsive in nature. The ground state of the anion also shows a deep potential well in the vicinity of its equilibrium geometry. In contrast, the ground and excited states of the cation are very loosely bound. Charge transfer properties of each of these states are also analyzed to obtain an in-depth understanding of the interatomic interactions. We found that the core–valence correlation has a substantial effect on the calculated spectroscopic constants.

KEYWORDS
charge-transfer, core–valence correlation, MRCI-F12, potential energy curves, spectroscopy

1 | INTRODUCTION

Extensive theoretical investigations within academic literature have delved deeply into diatomic compounds labeled as MX, wherein alkaline metals (M), with a particular emphasis on lithium and sodium, are paired with elements from group 15 (X). For instance, ab initio characterizations of the lowest-lying electronic states of diatomic systems have been performed in straightforward homologous systems, including hydrides like NH, PH, and AsH, as well as radical species such as nitrenes (NaN, KN), phosphinidines (NaP, LiP), and arsinidenes (NaAs, LiAs). In the context of the lithium series, rigorous ab initio calculations at a high level have specifically addressed the isovalent radicals LiN [1–4], LiP [4–6], and LiAs [7], elucidating their lowest-energy electronic states. To the best of our knowledge, there have been no reported experimental results for these three diatomic compounds. Consequently, these studies provide a reliable and comprehensive perspective on their potential energy profiles and associated spectroscopic parameters.

Numerous theoretical studies of alkali metal hydrides and halides have been widely conducted and are readily accessible in the literature. For instance, Yuan et al. have examined the electronic structure of the X^2A state of Li_2H [8]. Similarly, Yang et al. investigated the potential energy curves of NaH [9], demonstrating that for the ground state, the electronic state is $X^1\Sigma^+$, whereas for the first excited state, the electronic state is

$B^1\Pi$. Ab initio calculations have also been performed for other hydrides, including KH [10], RbH [11], and CsH [12], whereas alkali metal halides have also garnered considerable attention. In general, the work reported by Bernath et al. and Garcia-Cuesta et al. has yielded a number of significant contributions for understanding diatomic systems [13–15]. On the other hand, diatomic molecules containing a Li atom, such as NaLi [16], LiRb [17], LiO [18], etc., have a particular interest as their formation at ultracold temperatures often involves a barrierless PEC in its entrance channel [19].

Nitrenes are molecules having an N—R bond, with imidogen (NH) being the simplest system, which, in contrast to LiN (i.e., the next simpler nitrene system), is well studied. The initial investigation of LiN, conducted by Dykstra et al. [1], utilized the configuration interaction with singles and doubles (CISD) approach to delineate the $X^3\Sigma^-$ and $A^3\Pi$ electronic states. Subsequently, Matsika et al. [2] expanded on this analysis by predominantly employing the complete active space self-consistent field (CASSCF) method to further characterize the electronic states of LiN. Margrave et al. were among the pioneers in determining the bond dissociation energy of the LiN experimentally, reporting a value that range from 4.8 to 7.1 eV [20]. However, subsequent experiments revealed a significantly smaller bond dissociation energy of approximately 2.2 eV [21]. Interestingly, Matsika et al. pointed out that even this reduced value is overestimated by approximately 0.4–0.6 eV [2]. In 1974, Schaefer III et al. conducted CISD study of the LiN molecule and calculated the $^3\Sigma^-$ and $^3\Pi$ electronic states [1]. Their findings reported a dissociation energy of 0.85 eV for the $^3\Sigma^-$ state, which was significantly lower than the experimental reports. Khait et al. examined seven lower-lying states of the LiN molecule using SCF-DZ level calculations, concluding that the ground $^3\Sigma^-$ state is not bound [22]. Subsequently, in 1993, Simons and colleagues performed ab initio calculations using the MP2, MP4, and QCISD methods on neutral LiN as well as its cationic and anionic counterparts [4]. Their results indicate a bond dissociation energy of 1.5 eV, which is closely aligned with the experimental findings. Matsika and co-workers utilized the MR-CISD level to calculate the potential energy curves and spectroscopic constants for the ground state and various excited states [2]. More recently, Ishii et al. [3] enhanced the level of correlation treatment and provided a characterization of the two lowest states using the internally contracted multi-reference configuration interaction (MRCI) technique.

The results obtained from ab initio calculations reported in the existing literature exhibit inconsistencies, primarily stemming from the utilization of various methods. Furthermore, these calculations often omit core–valence correlations and relativistic effects, which are potentially significant factors in accurately determining the electronic structure of both ground and excited states. This situation underscores the need for additional computational endeavors. Additionally, it is worth noting that no theoretical investigations into the potential energy curves (PECs) have been undertaken for LiN^+ and LiN^- ions.

In this study, we examine the electronic states, both ground and excited, of the LiN molecule and its ions. To achieve this, we employ the MRCI-F12 + Q method, additionally incorporating scalar relativistic corrections and core–valence correlation, rendering it highly regarded for its accuracy [23]. Dipole moment analysis is also carried out to evaluate the charge transfer between the two atoms of the systems and analyze the transition dipole moment between two electronic states. The spectroscopic parameters and the energies of bound vibrational states are also determined and reported here.

2 | COMPUTATIONAL DETAILS

The diatomic molecule LiN, along with its cation (LiN^+) and anion (LiN^-), have been examined, and the potential energy curves (PECs) have been extrapolated from calculations extending to the dissociation limits. The methodology employed for our work is the explicitly correlated multi-reference configuration interaction [24–26], incorporating Davidson correction (MRCI-F12 + Q) [27]. The core–valence correlation effects and scalar relativistic corrections using the second-order Douglas–Kroll–Hess (DKH) Hamiltonian are also considered in this study. The energy convergence of all calculations is 1.0×10^{-8} Hartree. All ab initio calculations have been performed using MOLPRO software [28]. Three types of correlation consistent quintuple-ζ basis set has been chosen in order to capture the effects of core–valence correlation and relativistic effects, viz., aug-cc-pV5Z (AV5Z), aug-cc-pCV5Z (ACV5Z), and aug-cc-pV5Z-DK (ACV5Z-DK). Moreover, a similar set of correlation consistent triple-ζ (AVTZ) and quadruple-ζ (AVQZ) basis sets have been employed to evaluate basis set convergence.

In this work, the electronic states of the linear LiN systems are labeled in terms of irreducible representations of the Abelian C_{2v} point group. The Li and N collisional channel is described in such a way that the N atom is held at the center of the coordinate frame, while the Li atom is allowed to approach from the z-axis at a distance R. The PECs for Li and N interaction have been generated starting from the asymptotic region ($R = 7.0$ Å) to compact geometries ($R = 0.5$ Å) with a step size of 0.05 Å. Initial ab initio calculations are performed with the complete active space self-consistent field (CASSCF) [29, 30] approach to obtain references for the more precise MRCI calculations. The active space for CASSCF calculation includes five (LiN^+), six (LiN), and seven (LiN^-) valence electrons in eight molecular orbitals (MOs), viz., the 2s and three 2p orbitals of both atoms ($4a_1$, $2b_1$, $2b_2$), that is, [CAS(5,8)], [CAS(6,8)], and [CAS(7,8)], respectively. The correlated electrons are the 2s and 2p electrons of N and the valence electron of the Li atom. The 1s electrons of both atoms do not take part in the construction of the active space but are correlated in the calculations with core–valence correlation (with ACV5Z basis set) and scalar relativistic effect calculations (with ACV5Z-DK basis set). At the CASSCF level, the total number of configuration state functions (CSFs) for the neutral LiN system is ∼380 (triplet spin states) and ∼110 (quintet spin states), while that for the LiN^+ system is ∼250 (doublet spin states) and ∼140 (quartet spin states). The ground quartet state of LiN^- has

352 CSFs. At the MRCI level, the total number of contracted configurations with AV5Z basis set lie within 5×10^5 to 1×10^6 and fall within 3×10^6 to 5×10^6 for the calculations when core–valence correlation effects are taken into account. One should note that for the neutral system, state-averaged CASSCF (SA-CASSCF) calculations have been performed over all electronic states considered in this study. On the other hand, SA-CASSCF calculations are performed on $^2\Sigma^-$ and $^2\Delta$ states, and on $^4\Sigma^-$ and $^2\Pi$ states separately, for the cationic system. For better convergence, one additional $^4\Delta$ state has been included in the SA-CASSCF calculation for the determination of the ground state ($^4\Sigma^-$) of LiN^-.

The dipole moment is evaluated as the expectation value of the dipole moment operator in the electronic state normalized wave function, given by:

$$\langle \mu \rangle = \left\langle \Psi \left| \sum_{i=1}^{N} q_i r_i \right| \Psi \right\rangle \tag{1}$$

where the summation runs over all the charged particles N (electrons and nuclei), with $\boldsymbol{r}_i$ being the position vector of charge q_i, and Ψ the normalized wave function. One can calculate the effective charge Q_{eff} on each atomic center from the component μ_z of the dipole moment along the z-axis as:

$$Q_{\text{eff}} = \frac{\mu_z}{R} \tag{2}$$

Adhering to the standard sign convention [31], a negative Q_{eff} charge on the Li atom corresponds to a negative value of μ_z, that is, when the dipole moment is directed toward the N atom. Since the dipole moment of an electrically charged species is not invariant under the choices of the coordinate frame, the variation of Q_{eff} with respect to R has been computed by positioning the N atom at the origin of the coordinate frame. The dipole moment μ_z will then solely depend on the distance R and the charge of the Li atom. Mulliken population analysis has been performed along the PECs, and the obtained charges are compared with the Q_{eff} of Li. Note that it is conventional to determine the dipole moments at the center of mass (COM), and therefore, the μ_z values reported in this work are calculated at the COM.

To find the equilibrium bond length (r_e), a five-point fit of the PEC around the minimum energy has been performed using weighted least squares approach [32] as incorporated in the PSI-4 package [33]. Once r_e is determined, second-order vibrational perturbation theory is applied to obtain other spectroscopic constants, such as the harmonic vibrational frequency (ω_e), anharmonic frequency term ($\omega_e x_e$), and rotational constants (B_e, α_e). The CASSCF wavefunctions have been utilized to evaluate the spin-orbit constant at the equilibrium geometry using the Breit-Pauli operator [34] for the base electronic state. Finally, the rovibrational energy levels of the bound electronic states of $LiN^{\pm1,0}$ have been calculated by the LEVEL16 program developed by Le Roy [35].

3 | RESULTS AND DISCUSSIONS

3.1 | LiN neutral molecule

In accordance with the atomic term symbols of Li and N atoms, two molecular states arises from the coupling between Li (^2S_g) + N (^4S_u) and Li (^2P_u) + N (^4S_u) terms. Note that the molecular states arising from the coupling between Li and the first excited state of N (^2D_u) are not considered in this study. The molecular term symbols corresponding to both are reported in Table 1. The energy of the molecular state of the LiN molecule that arises from the coupling between Li (^2S_g) + N (^4S_u) atomic states at the asymptotic region ($R = 7.0$ Å) is considered as zero, whereas the energies of the other states are shifted relative to this electronic state. There is a remarkable concordance between the data obtained from experimental measurements and the calculated data obtained in this work for the first excited state, which demonstrates the efficacy of the computational method employed. It is also evident that the calculations involving core–valence correlations have marginally better agreement with the experimental results. Moreover, relativistic effects do not have any significant contribution to the relative energies at the asymptotic region.

The MRCI-F12 + Q/AV5Z PEC for the ground and excited states for the Li + N interaction with respect to distance R are depicted in Figure 1 and are also provided in the supplementary information (SI) file. As can be distinctly seen in Figure 1, each of the triplet states, that is, X $^3\Sigma^-$, A $^3\Pi$, and 2 $^3\Sigma^-$, are stable, they possess a relatively deep potential well, and there is no potential barrier in the PECs for these states. Therefore, these states may serve on the potential application in ultracold temperatures. The well-depth of the ground state is approximately 1.7 eV. However, the well-depth of the A $^3\Pi$ state is far more significant (≈3.3 eV). This state becomes almost degenerate with the X $^3\Sigma^-$ state at its equilibrium geometry. At the equilibrium geometry of the ground and the first excited state, that is, X $^3\Sigma^-$, A $^3\Pi$, the Li and N are found at a much shorter R (≈1.7–1.9 Å) than that found for the second excited 2 $^3\Sigma^-$ state ($R \approx 2.2$ Å). On the other hand, the potential well depth of the 2 $^3\Sigma^-$ state is much shallower (≈1.3 eV). Conversely, the quintet states, that is, 1 $^5\Sigma^-$, 1 $^5\Pi$, and 2 $^5\Sigma^-$, are repulsive in nature and are far from a Morse-type potential.

TABLE 1 Labelling of the lowest electronic states of $LiN^{\pm1,0}$ in the $C_{\infty v}$ point group and MRCI-F12 + Q energies relative to the ground state of Li + N in the asymptotic region (R = 7.0 Å).

	Molecular states	Relative energies/eV					
		Calc.[a]					
States	Λ-S states	AVTZ	AVQZ	AV5Z	ACV5Z	ACV5Z-DK	Exp.
$Li^+ (^1S_g) + N (^2D_u)$	$^2\Sigma^-, ^2\Pi, ^2\Delta$	7.7241	7.7072	7.6987	7.7484	7.7484	7.7752[b]
$Li^+ (^1S_g) + N (^4S_u)$	$^4\Sigma^-$	5.3345	5.3387	5.3407	5.3783	5.3783	5.3917[b]
$Li (^2P_u) + N (^4S_u)$	$^3\Sigma^-, ^3\Pi$	1.8402	1.8396	1.8393	1.8490	1.8490	1.8478[b]
	$^5\Sigma^-, ^5\Pi$	1.8414	1.8408	1.8405	1.8497	1.8497	1.8478[b]
$Li (^2S_g) + N (^4S_u)$	$^3\Sigma^-, ^5\Sigma^-$	0.0000	0.0000	0.0000	0.0000	0.0000	0.0000
$Li^- (^1S_g) + N (^4S_u)$	$^4\Sigma^-$	−0.5689	−0.5698	−0.5694	−0.5439	−0.5439	−0.6180[c]

Note: "Exp." and "Calc." refer to the experimental and calculated values. AVTZ, AVQZ, AV5Z, ACV5Z, and ACV5Z-DK refer to the different basis sets used in the calculations.

[a]Weighted average over the same spin states.

[b]Data taken from Reference [36].

[c]Data taken from Reference [37].

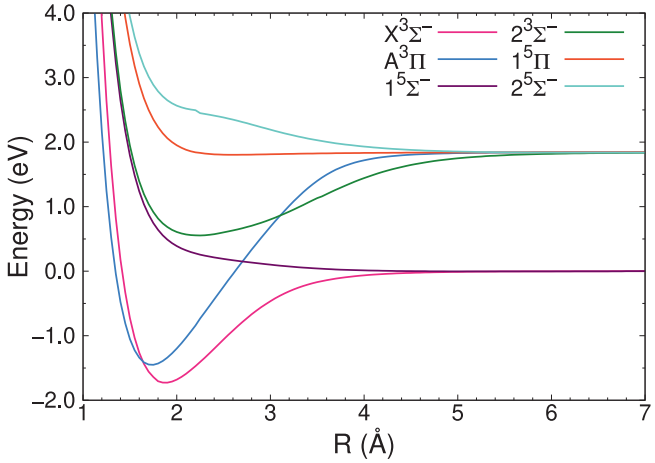

FIGURE 1 Potential energy curves (PECs) of the lower lying triplet and quintet states of the LiN molecule, calculated at the MRCI-F12 + Q/AV5Z level. R is the distance between N and Li in Å. Energy is in eV, with respect to the asymptotic energy (at R = 7.0 Å) of the X $^3\Sigma^-$ state.

The variation of the z-component of the dipole moment, μ_z, and the effective charge, Q_{eff}, with R, are illustrated in Figure 2A,B, respectively. For comparison, the Mulliken charges are also plotted in Figure 2B. These figures may furnish valuable insights into the charge-transfer in various states of the LiN molecule. From Figure 2A, it can be clearly seen that as the two atoms approach each other, the μ_z values deviate from zero, found at the asymptotic region, which is suggestive of charge separation. This is true for each of the three bound states. For the ground X $^3\Sigma^-$ state and the first excited A $^3\Pi$ state, at $R \approx 4.5$ Å, the μ_z values start to become positive, suggesting that the Li atom has partial positive charge, while the N atom is negatively charged, according to the sign convention used in this work. At around $R \approx 2.5$ Å for the X $^3\Sigma^-$ and $R \approx 3.0$ Å for the A $^3\Pi$ state, the μ_z values reach maximum positive values and then start to decrease with the decrease in R. On the other hand, for the 2 $^3\Sigma^-$ state, μ_z values are positive even at larger R (≈6.0 Å), attain maximum at R (≈3.5 Å) and become negative for shorter R (<3.0 Å). The variation of Q_{eff} and Mulliken charges on Li atom with R not only corroborate with each other but also have good agreement with the changes in μ_z values. It is evident from Figure 2B that there is a charge transfer from Li to N between the ground state, X $^3\Sigma^-$, and the first excited state, A $^3\Pi$. In contrast, for the bound 2 $^3\Sigma^-$ state, there is a charge transfer from the N atom to the Li atom, initiated around 3.0 Å. One should note that the effective charge model at shorter distances ($R \leq 2.0$ Å) is not valid since the center of positive or negative charges is not well defined [38].

Figure 3 exhibits the obtained values for the transition dipole moment, μ_T, along the internuclear distance R of the LiN molecule between states X $^3\Sigma^- \rightarrow$ A $^3\Pi$, X $^3\Sigma^- \rightarrow$ 2 $^3\Sigma^-$, and A $^3\Pi \rightarrow$ 2 $^3\Sigma^-$. If the integral defining the transition dipole moment is not equal to zero, the transition between states is allowed. The variation of μ_T with respect to R for the X $^3\Sigma^- \rightarrow$ A $^3\Pi$, X $^3\Sigma^- \rightarrow$ 2 $^3\Sigma^-$ transitions are very similar; they are almost constant till 3.0–3.5 Å (with $\mu_T \approx 6.0$ Debye) and starts to diminish rapidly with decreasing R. On the other hand, the transition probability from A $^3\Pi \rightarrow$ 2 $^3\Sigma^-$ is almost zero till 4.5 Å, which begins to increase as the distance between the atom decreases. The μ_T's at large atomic separation

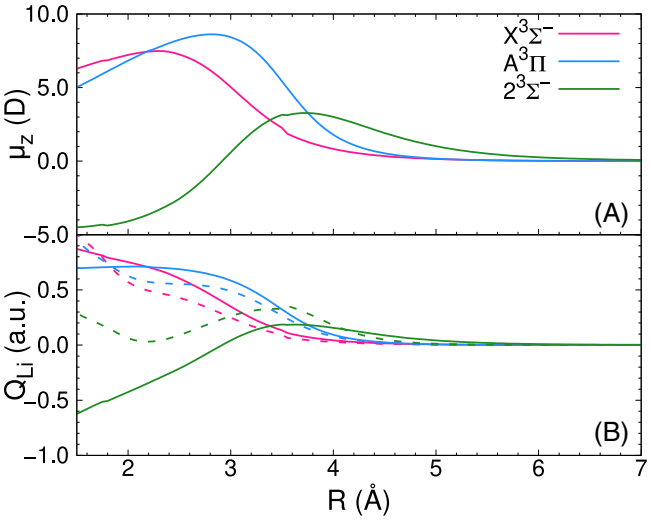

FIGURE 2 (A) Dipole moment, μ_z (in Debye) (B) Effective charge Q_{eff} (solid lines) and Mulliken charge (broken lines) on the Li atom as a function of R ($1.5 \le R \le 7.0$ Å) for the bound states of LiN molecule. The Q_{eff} values are determined by Equation (2), with μ_z calculated with Equation (1) at the MRCI-F12/AV5Z level.

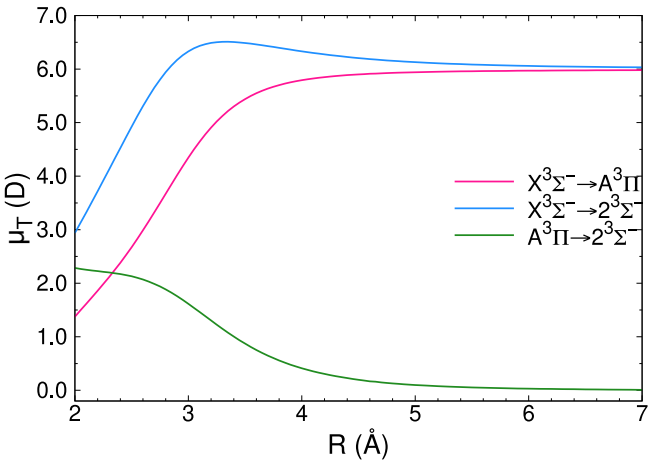

FIGURE 3 The transition dipole moment μ_T (Debye) for the (A) X $^3\Sigma^-$ → A $^3\Pi$ (B) X $^3\Sigma^-$ → 2 $^3\Sigma^-$ and (C) A $^3\Pi$ → 2 $^3\Sigma^-$ transitions along the internuclear distance R of the LiN molecule obtained at the MRCI-F12 level.

(R till 4.5 Å) may be attributed to the transitions between various states of the free Li atom. For example, the X $^3\Sigma^-$ → A $^3\Pi$ transition may be correlated with the ground ^{2}S state to the first excited ^{2}P transition in the Li atom (with $\mu_T \approx 6$ Debye).

We have calculated the spectroscopic constants for the bound electronic states, as detailed in the methodology section (Section 2), and are summarized in Table 2. The equilibrium bond lengths (r_e) of the bound electronic states do not change significantly with respect to the size of the basis set, that is, changing the basis set from AV5Z to AVQZ or AVTZ. For example, for the ground X $^3\Sigma^-$ state, the r_e remains almost constant at 1.88 Å for each of the basis sets. However, when core–valence correlation effects are considered, the r_e values slightly decrease. This is true for each of the bound states considered in this study. Moreover, we also find that the relativistic has no effect on the equilibrium bond distances. The dissociation energy (D_e) for each of the states, which is calculated as the difference in energy at asymptote and at r_e, shows that as the size of the basis set increases, there is an increase in the value of D_e. In other words, the potential well-depth in the PEC increases with the size of the basis set. The inclusion of core–valence correlation increases the D_e values for each of the $^3\Sigma^-$ states but decreases the same for the A $^3\Pi$ state. The relativistic effect seems to marginally lower the D_e values for the ground and first excited state.

From the vertical excitation energy (T_e) values in Table 2, we can see that the first excited state, A $^3\Pi$, lies relatively close to the ground state (≈0.4 eV), while that for the 2 $^3\Sigma^-$ state is around 2.4 eV. With the increase in size of the basis set, T_e values tend to increase. On the other hand, core–valence correlation and relativistic effect slightly decrease the same. Another important parameter is the harmonic vibrational frequency

TABLE 2 Spectroscopic constants of the bound electronic states of LiN molecule calculated by MRCI-F12 + Q method at the equilibrium bond length, r_e, (in Å). E_e is the total electronic energy (in Hartree), D_e is dissociation energies (in eV), T_e is the excitation energies (in eV), B_e and α_e are the rotational constants (in cm^{-1}), ω_e is the harmonic wavenumber (in cm^{-1}), $\omega_e x_e$ is the anharmonic term (in cm^{-1}), $<\mu>_e$ is the equilibrium dipole moment (in Debye), and A_{SO} spin-orbit constant at equilibrium (in cm^{-1}).

State	Basis set	r_e	E_e	D_e	T_e	B_e	ω_e	$\omega_e x_e$	α_e	$<\mu>_e$	A_{SO}
$2\ ^3\Sigma^-$	AVTZ	2.230	−61.9391	1.2717	2.3974	0.7253	291.4819	10.0721	0.0139	−3.4998	-
	AVQZ	2.232	−61.9417	1.2804	2.4241	0.7240	291.4532	14.0387	0.0112	−3.5168	-
	AV5Z	2.234	−61.9427	1.2800	2.4390	0.7223	290.0758	15.3110	0.0101	−3.5248	-
	ACV5Z	2.199	−62.0604	1.2908	2.4524	0.7456	300.1242	7.1417	0.0143	−3.7113	-
	ACV5Z-DK	2.199	−62.0926	1.2934	2.4486	0.7460	300.1249	6.8011	0.0145	−3.7054	-
	(MR-CISD/AVTZ)[b]	(2.194) [b]	(−61.9162)[c]	(1.162) [b]	(1.982) [b]	-	(434.93) [b]	(1.10) [b]	(0.094) [b]	-	-
$A\ ^3\Pi$	AVTZ	1.732	−62.0111	3.2385	0.3676	1.2026	776.2052	7.2632	0.0177	6.0885	−27.41
	AVQZ	1.732	−62.0149	3.2807	0.3773	1.2015	773.0941	7.3620	0.0178	6.0867	−28.06
	AV5Z	1.733	−62.0164	3.2940	0.3809	1.2013	772.5728	7.3826	0.0178	6.0903	−28.34
	ACV5Z	1.701	−62.1290	3.1652	0.3685	1.2466	821.3407	5.9408	0.0169	5.9363	−28.34
	ACV5Z-DK	1.701	−62.1609	3.1596	0.3690	1.2470	821.3107	5.9449	0.0169	5.9355	−28.39
	(MP2/6-311+G*)[a]	(1.728)[a]		-	-	-	(787) [a]	-	-	-	-
	(MR-CISD/AVTZ)[b]	(1.772) [b]	(−61.9771)[b]	(2.801) [b]	(0.324) [b]	-	(731.2) [b]	(6.45) [b]	(0.0170) [b]	-	-
$X\ ^3\Sigma^-$	AVTZ	1.877	−62.0216	1.6806	-	1.0236	663.7943	7.662	0.0166	6.9893	-
	AVQZ	1.876	−62.0251	1.7148	-	1.0245	665.2165	7.6152	0.0165	7.0032	-
	AV5Z	1.876	−62.0266	1.7283	-	1.0249	666.2194	7.5977	0.0164	7.0057	-
	ACV5Z	1.859	−62.1451	1.7512	-	1.0428	670.3432	5.9178	0.0208	6.8344	-
	ACV5Z-DK	1.859	−62.1771	1.7480	-	1.0427	670.0389	5.5437	0.0207	6.8301	-
	(MP2/6-311+G*)[a]	(1.874) [a]		(1.51) [a]	-	-	(681) [a]	-	-	-	-
	(MR-CISD/AVTZ)[b]	(1.921)[b]	(−61.9890)[b]	(1.279)[b]	-	-	(619.9) [b]	(7.07) [b]	(0.0165) [b]	(7.15) [b]	-

[a]Data taken from Reference [4].
[b]Data taken from Reference [2].

(ω_e). The values of ω_e for the first two bound states are markedly larger (664–821 cm^{-1}) than the 2 $^3\Sigma^-$ state (≈300 cm^{-1}). It is also evident that core–valence correlation has a much more significant effect on the spectroscopic constants, such as the ω_e, $\omega_e x_e$, B_e, and α_e, than the relativistic effect and size of the basis set. For example, the ω_e and B_e and α_e values increase significantly when the core–valence correlation effects are taken into account, except for the α_e values of the A $^3\Pi$ state which decrease. From the dipole moment ($<\mu>_e$) values at the equilibrium bond lengths, one can get glimpses into the induced atomic charges as well as their separation in the molecule. Among the bound states, in the ground X $^3\Sigma^-$, and the first excited A $^3\Pi$ state has a large positive value of $<\mu>_e$, which is suggestive of the partial negative charge residing on the N atom according to the sign convention used in this work. The opposite is true for the 2 $^3\Sigma^-$ state. Finally, we have found 25, 22, and 24 vibrational states for the X $^3\Sigma^-$, A $^3\Pi$, and 2 $^3\Sigma^-$ states that fall below their respective dissociation limit (see Supporting information S1).

The results obtained in this work are compared with those reported by Boldyrev et al. [4] as well as Matsika et al. [2]. In general, there is a good agreement between the results found in this work and previously reported values (see Table 2). The equilibrium bond lengths in X $^3\Sigma^-$ and A $^3\Pi$ states reported in this work have better agreement with those reported by Boldyrev et al. In contrast, the r_e values reported by Matsika et al. are slightly larger. Moreover, the differences in many spectroscopic constants with both those previous reports can be attributed to the fact that in this study, core–valence and relativistic effects have been taken into account.

Dominant electronic configurations and the weights of the leading CI coefficients of the electronic states of LiN are reported in Table 3. Calculations reveal that the electronic ground state for the LiN molecule, that is, X $^3\Sigma^-$ state, corresponds to the valence electron configuration of $(3\sigma)^2(4\sigma)^2(1\pi)^2$, where the two π electrons have the same spin magnetic quantum number. The first bound excited state was obtained from the electron transfer from the 4σ orbital to the 1π orbital with an excitation energy of around 0.4 eV, representing the A $^3\Pi$ electronic state. Similarly, the second bound excited state, 2 $^3\Sigma^-$, has been obtained by electron promotion from the 4σ orbital to the 5σ orbital with an excitation energy of around 2.4 eV. From the CI weights of the X $^3\Sigma^-$ and A $^3\Pi$ states, it is evident that they essentially have a single-reference character. However, the 2 $^3\Sigma^-$ state has some multi-reference characters stemming from different spin magnetic quantum numbers of the electrons in the 5σ and 1π orbitals.

Finally, the vertical (V) and adiabatic (A) ionization potential (IP) and electron affinity (EA) of the LiN molecule are also provided in Table 4. As expected, the VIP values are slightly larger (≈7.0 eV) than the corresponding AIPs (≈6.8–6.9 eV). In contrast, the VEA values (0.40–0.42 eV) are marginally smaller than the corresponding AEA values (0.42–0.44 eV). Increases in the size of the basis set and core–valence correlation effect increase the corresponding VIP and AIP values, while the relativistic effect tends to decrease them slightly. While we have found no correlation between the size of the basis set and relativistic effects with the VEA or AEA values, core–valence correlation effects decrease the electron affinities by around 0.02 eV.

TABLE 3 Dominant electronic configurations and the weights of the leading CI coefficients of the electronic states of $LiN^{\pm1,0}$ at the equilibrium geometry.

Species	State	Electronic configuration	CI weights
LiN^+	1 $^2\Delta$	$(3\sigma)^2(4\sigma)^1(1\pi)^2$	0.720
	1 $^2\Sigma^-$	$(3\sigma)^2(4\sigma)^1(1\pi)^2$	0.716
	A $^2\Pi$	$(3\sigma)^2(4\sigma)^2(1\pi)^1$	0.803
	X $^4\Sigma^-$	$(3\sigma)^2(4\sigma)^1(1\pi)^2$	0.959
LiN	2 $^3\Sigma^-$	$(3\sigma)^2(4\sigma)^1(5\sigma)^1(1\pi)^2$	0.531
	A $^3\Pi$	$(3\sigma)^2(4\sigma)^1(1\pi)^3$	0.919
	X $^3\Sigma^-$	$(3\sigma)^2(4\sigma)^2(1\pi)^2$	0.892
LiN^-	X $^4\Sigma^-$	$(3\sigma)^2(4\sigma)^2(5\sigma)^1(1\pi)^2$	0.933

TABLE 4 Vertical (V) and adiabatic (A) ionization potential (IP) and electron affinity (EA) of LiN molecule (in eV) calculated at the MRCI-F12 + Q level.

Basis set	VIP	AIP	VEA	AEA
AVTZ	6.9756	6.8109	0.4227	0.4463
AVQZ	7.0148	6.8490	0.4191	0.4408
AV5Z	7.0310	6.8653	0.4218	0.4435
ACV5Z	7.0713	6.9088	0.4063	0.4245
ACV5Z-DK	7.0684	6.9061	0.4052	0.4245

3.2 | $LiN^{\pm}$ cation and anion

The electronic states for $LiN^{\pm}$ ionic species have been scrutinized utilizing MRCI-F12 + Q calculations. For the LiN^{+} cation, three doublet states and one quartet state were investigated, encompassing X $^4\Sigma^-$, A $^2\Pi$, 1 $^2\Delta$ and 1 $^2\Sigma^-$ states. Conversely, only one quartet state, X $^4\Sigma^-$, has been examined for LiN^- anion that arises from the coupling between ^1S_g of Li^- and ^4S_u of N atoms. The dissociation limit for each of the states of the LiN^+ molecule has an excellent agreement with the experimental observation (see Table 1). The calculated values have much better agreement with the experimental results when core–valence correlation effects are considered. The size of the basis set, as well as the relativistic effect, has minimal impact on the calculated relative energies. The X $^4\Sigma^-$ state of the LiN^- molecule at its dissociation limit has slightly larger energies (−0.57 to −0.54 eV) than the experimental observation (−0.62 eV). This is due to the fact that the MRCI method is not size-consistent, that is, the energy of the constituting species (such as atoms) of a molecule at large separation is different to the sum of the energies of the constituting species calculated in isolation [39]. The above statement can be verified from the fact that when calculated in isolation, the electron affinity of the Li atom with ACV5Z basis set is found to be −0.617 eV, which is very close to the experimentally reported value (−0.618 eV).

The PECs of the lowest electronic states of LiN^+ and LiN^- are illustrated in Figures 4 and 5, respectively. Except for the A $^2\Pi$ state, all other electronic states of LiN^+, that is, X $^4\Sigma^-$, 1 $^2\Delta$ and 1 $^2\Sigma^-$ states, all have very shallow potential wells (∼ 0.2 eV), and therefore, they have very moderate stability (see D_e values in Table 5). The A $^2\Pi$ state, on the other hand, is relatively more stable. The r_e and D_e values of X $^4\Sigma^-$ state for LiN^+ have a good agreement with the MP2/6-311+G* results obtained by Boldyrev et al. (0.2 eV) [4]. Similarly, the equilibrium bond length in the A $^2\Pi$ state obtained in this study is very close to that reported by Boldyrev et al. [4]. For the X $^4\Sigma^-$ of the anionic LiN^- molecule, although there is an excellent agreement in the r_e values with that of Boldyrev et al. (≈1.9 Å), the dissociation energy apparently underestimated in that study (1.6 eV

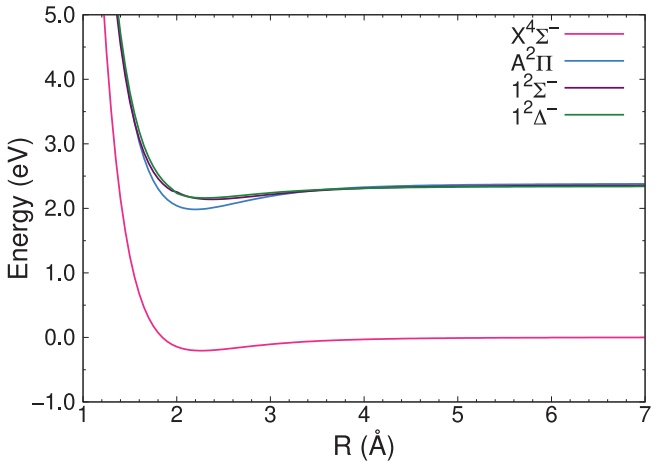

FIGURE 4 Potential energy curves (PECs) of the lower lying doublet and quartet states of the LiN^+ molecule, calculated at the MRCI-F12 + Q/AV5Z level. *R* is the distance between N and Li in Å. Energy is in eV, with respect to the asymptotic energy (at $R = 7.0$ Å) of the X $^4\Sigma^-$ state.

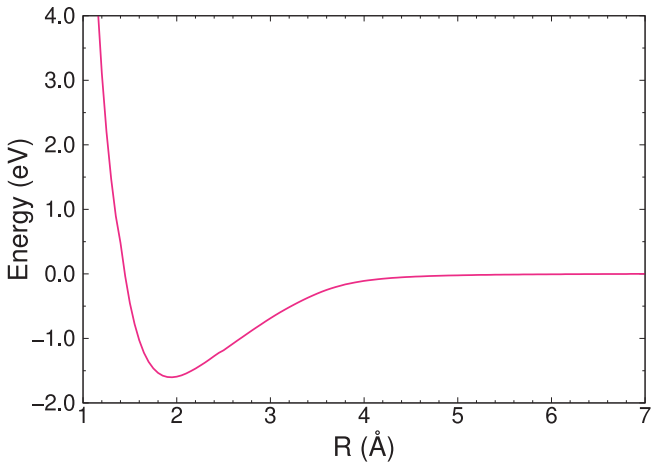

FIGURE 5 Potential energy curve (PEC) of the ground quartet state of the LiN^- molecule, calculated at the MRCI-F12 + Q/AV5Z level. *R* is the distance between N and Li in Å. Energy is in eV, with respect to the asymptotic energy (at $R = 7.0$ Å).

TABLE 5 Spectroscopic constants of the lowest electronic states of LiN^+ molecule calculated by MRCI-F12 + Q method at the equilibrium bond length, r_e, (in Å). E_e is the total electronic energy (in Hartree), D_e is dissociation energies (in eV), T_e is the excitation energies (in eV), B_e and α_e are the rotational constants (in cm^{-1}), ω_e is the harmonic wavenumber (in cm^{-1}), $\omega_e x_e$ is the anharmonic term (in cm^{-1}), $<\mu>_e$ is the equilibrium dipole moment (in Debye) calculated at the center of mass, and A_{SO} spin-orbit constant at equilibrium (in cm^{-1}).

State	Basis set	r_e	E_e	D_e	T_e	B_e	ω_e	$\omega_e x_e$	α_e	$<\mu>_e$	A_{SO}
$1\,^2\Delta$	AVTZ	2.300	−61.6833	0.1790	2.3961	0.6819	237.0611	13.3900	0.0343	6.4434	−3.22
	AVQZ	2.300	−61.6861	0.1786	2.3769	0.6815	235.7974	10.6357	0.0351	6.4383	−3.30
	AV5Z	2.301	−61.6874	0.1784	2.3664	0.6812	236.1228	12.4758	0.0344	6.4412	−3.30
	ACV5Z	2.263	−61.8042	0.1916	2.3666	0.7044	248.0544	10.3378	0.0353	6.2870	−3.31
	ACV5Z-DK	2.263	−61.8364	0.1934	2.3658	0.7043	247.9307	10.3707	0.0352	6.2872	−3.31
$1\,^2\Sigma^-$	AVTZ	2.373	−61.6841	0.2159	2.3808	0.6404	230.0434	7.3795	0.0279	6.6980	-
	AVQZ	2.373	−61.6869	0.2155	2.3617	0.6402	229.9046	7.1596	0.0276	6.6936	-
	AV5Z	2.373	−61.6882	0.2154	2.3516	0.6403	229.8948	7.2709	0.0276	6.6931	-
	ACV5Z	2.338	−61.8051	0.2285	2.3498	0.6600	239.4402	8.2756	0.0280	6.5643	-
	ACV5Z-DK	2.338	−61.8372	0.2276	2.3488	0.6599	239.3628	8.2578	0.0280	6.5639	-
$A\,^2\Pi$	AVTZ	2.201	−61.6897	0.3971	2.2252	0.7442	343.6599	11.0845	0.0249	6.0527	−52.84
	AVQZ	2.201	−61.6926	0.3954	2.2037	0.7444	342.8266	9.4763	0.0249	6.0477	−54.06
	AV5Z	2.200	−61.6939	0.3945	2.1921	0.7448	343.2267	9.4852	0.0249	6.0441	−54.70
	ACV5Z	2.169	−61.8110	0.4594	2.1853	0.7664	361.1670	8.6543	0.0241	5.9248	−54.82
	ACV5Z-DK	2.169	−61.8431	0.4587	2.1843	0.7664	361.1055	8.6400	0.0241	5.9240	−54.94
	(MP2/6-311+G*)[a]	(2.173)[a]	-	-	-	-	(393)[a]	-	-	-	-
$X\,^4\Sigma^-$	AVTZ	2.258	−61.7713	0.2037	-	0.7070	255.4789	11.1297	0.0351	6.3056	-
	AVQZ	2.258	−61.7734	0.2041	-	0.7071	255.6451	10.5381	0.0348	6.2996	-
	AV5Z	2.258	−61.7743	0.2032	-	0.7070	255.4373	10.5666	0.0348	6.2987	-
	ACV5Z	2.224	−61.8912	0.2200	-	0.7292	267.7870	10.1116	0.0349	6.1557	-
	ACV5Z-DK	2.224	−61.9233	0.2197	-	0.7291	267.5834	10.097	0.0349	6.1562	-
	(MP2/6-311+G*)[a]	(2.243)[a]		(0.2081)[a]			(267)[a]				

[a]Data taken from Reference [4].

TABLE 6 Spectroscopic constants of the ground electronic state of LiN^- molecule calculated by MRCI-F12 + Q method at the equilibrium bond length, r_e, (in Å). E_e is the total electronic energy (in Hartree), D_e is dissociation energies (in eV), B_e and α_e are the rotational constants (in cm^{-1}), ω_e is the harmonic wavenumber (in cm^{-1}), $\omega_e x_e$ is the anharmonic term (in cm^{-1}), and $<\mu>_e$ is the equilibrium dipole moment (in Debye) calculated at the center of mass.

State	Basis set	r_e	E_e	D_e	B_e	ω_e	$\omega_e x_e$	α_e	$<\mu>_e$
$X^4\Sigma^-$	AVTZ	1.941	−62.0380	1.5576	0.9571	576.3381	7.5453	0.0187	−7.2146
	AVQZ	1.939	−62.0413	1.5854	0.9589	577.9447	7.5980	0.0187	−7.5719
	AV5Z	1.939	−62.0429	1.6021	0.9592	580.0272	9.5669	0.0176	−7.6765
	ACV5Z	1.921	−62.1607	1.6314	0.9782	589.1281	3.5396	0.0183	−7.8239
	ACV5Z-DK	1.921	−62.1927	1.6282	0.9782	588.8058	3.5281	0.0183	−7.8251
	(MP2/6-311+G*)[a]	(1.932)[a]		(1.3616)[a]		(593)[a]			

[a]Data taken from Reference [4].

vs. 1.4 eV, see Table 6). Finally, and more interestingly, none of these states (for both $LiN^{\pm}$) possess a barrier leading to the formation of the bound states. Therefore, similar to the neutral LiN, the ionic variants could also be exploited at low temperatures.

The prominent reason for the modest stabilization for each of the bound states of the LiN^+ molecule may be due to the small N to Li charge transfer as both atoms approach each other (see Figure 6B for Q_{eff} and Mulliken charges). This N to Li charge transfer takes place around the equilibrium bond length (2.3–3.0 Å). Note that the Q_{eff} and Mulliken charges follow an opposite trend for shorter R (≤2.3 Å); Q_{eff} values show that the Li atom would gain electron density from the N atom, while the Mulliken charges demonstrate that Li atom progressively inherits more partial positive charges as R decreases. In contrast, the ground state of LiN^- is stabilized more extensively by an amount of ∼1.6 eV. The variation of Q_{eff}

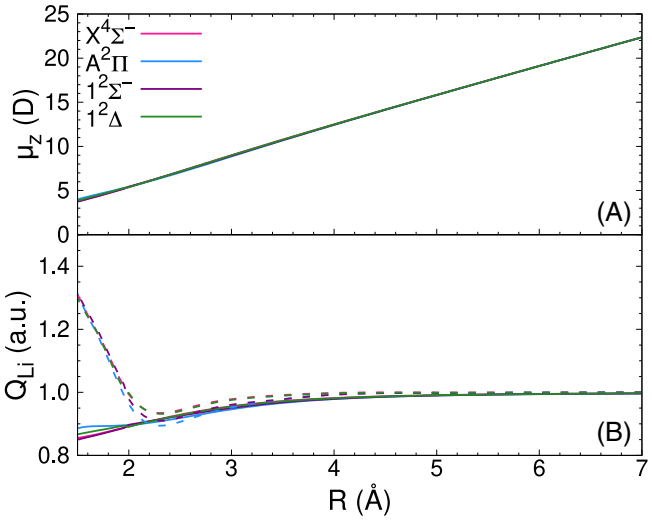

FIGURE 6 (A) Dipole moment, μ_z (in Debye) (B) Effective charge Q_{eff} (solid lines) and Mulliken charges (broken lines) on the Li atom as a function of R ($1.5 \le R \le 7.0$ Å) for the bound states of LiN^+ molecule. The Q_{eff} values are determined by Equation (2), with μ_z calculated with Equation (1) at the MRCI-F12/AV5Z level. The μ_z values reported in (A) are calculated at the center of mass.

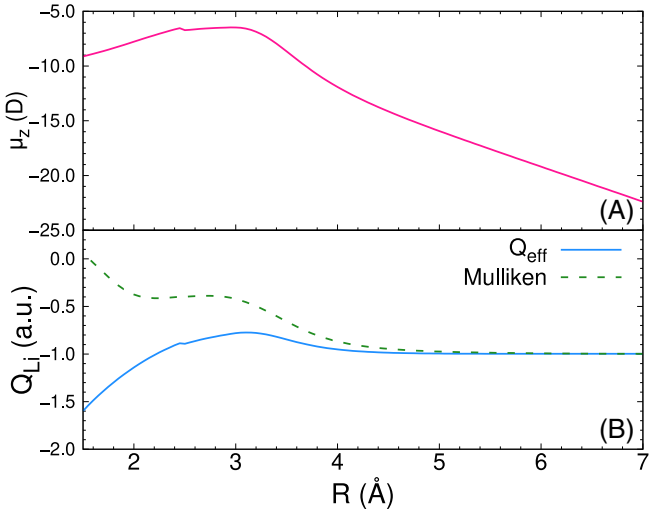

FIGURE 7 (A) Dipole moment, μ_z (in Debye) (B) Effective charge Q_{eff} (solid lines) and Mulliken charges (broken lines) on the Li atom as a function of R ($1.5 \le R \le 7.0$ Å) for the ground state of LiN^- molecule. The Q_{eff} values are determined by Equation (2), with μ_z calculated with Equation (1) at the MRCI-F12/AV5Z level. The μ_z values reported in (A) are calculated at the center of mass.

and Mulliken charges on the Li atom with the distance R is very interesting for the X $^4\Sigma^-$ state of LiN^- (see Figure 7B). At larger distances (within $4.5 \le R \le 7.0$ Å), there is no charge transfer between the atom; within $R = 3.0$–4.5 Å, there is Li to N atom charge transfer, as verified by both models. Below 3.0 Å distance, Mulliken charges show that Li to N charge transfer will continue to take place, while the Q_{eff} values indicate the opposite.

The electronic configurations of the electronic states of LiN^+ and LiN^- are tabulated in Table 3. All states are found to be predominantly single reference ones. The spectroscopic constants of these ions are provided in Tables 5 and 6. The equilibrium bond distance for the bound cationic states are found to be larger (2.2–2.3 Å) than the anionic state (~1.9 Å). Due to the shallow depth of the potential well surrounding the equilibrium geometry of the cations, their vibrational frequency (~230–360 cm^{-1}) is much smaller compared to the anion (~580 cm^{-1}). The vibrational frequency reported for the X $^4\Sigma^-$ state of both LiN^+ and LiN^- matches reasonably well with those reported by Boldyrev et al. [4]. However, the ω_e value previously reported for the A $^2\Pi$ state of LiN^+ is slightly overestimated (361 vs. 393 cm^{-1}). On the other hand, the spin-orbit constant of the A $^2\Pi$ state of LiN^+ (−55 cm^{-1}) was found to be larger than that obtained for the A $^3\Pi$ state of the neutral LiN molecule (−28 cm^{-1}). Finally, the rovibrational energy levels for each of these states are provided in the supplementary information file S1. Note that only the first six

rotational energy levels are provided. The ground state of the anion has 29 vibrational energy levels that fall below its dissociation limit. On the other hand, only one bound vibrational state has been found for each of the bound states of the cation. This is due to the fact that the D_e for this state is relatively small.

Similar to the conclusion drawn on the neutral LiN molecule, the size of the basis set and relativistic effect do not have any significant effect on equilibrium bond length, dissociation energy or various spectroscopic parameters for the ionic variants (see Tables 5 and 6). However, the core–valence correlation effect seems to shorten the r_e and increase D_e values, that is, the well-depth in the PEC. This is true for each of the bound states of the ionic system considered in this study. On the other hand, the vertical excitation energies (T_e) of the LiN^+ states tend to decrease as the size of the basis set increases, as well as when core–valence correlations are considered. Similarly, the inclusion of core–valence correlation also increases the vibrational frequency ω_e, rotational constant, B_e.

4 | CONCLUSION

We have calculated the properties of the low-lying electronic states of neutral LiN and its ionic counterparts, that is, LiN^+ and LiN^-. We have employed a highly accurate multi-reference configuration interaction (MRCI) method, including Davidson correction coupled with a series of triple to quintuple-ζ basis functions. The explicit electron correlation (-F12), core–valence electron correlation and scalar relativistic effects have been taken into account. Computational results at the dissociative limit for each state of the neutral and ionic LiN molecule have good agreement with experimental values.

For the neutral LiN molecule, the triplet states are bound, while the quintet states are dissociative. Out of the bound triplet states, $^3\Sigma^-$ is the ground state, while the $^3\Pi$ is the first excited state that is highly stabilized. Our results also show that Li to N charge transfer plays a pivotal role in the stabilization of the bound states of LiN. The ground state of anionic LiN^- molecules is remarkably stabilized, justified by having a deep potential well due to Li to N charge transfer. In contrast, the ground and excited states of LiN^+ species are weakly bound, having dissociation energy of ~0.2–0.5 eV.

In addition to dissociation energies, we have also calculated many spectroscopic constants, such as excitation energies, rotational constants, harmonic and anharmonic wavenumber, dipole moment and spin-orbit constants, rovibrational energy levels, for all of the states at their equilibrium geometry and compared them to previously reported values. We found that the size of the basis set and scalar relativistic effect have no significant effect on the equilibrium bond lengths, dissociation energies or spectroscopic constants considered in this work. In contrast, core–valence correlation plays a pivotal role in the electronic properties. More specifically, when the core–valence correlation is taken into account, the equilibrium bond length between N and Li decreases, at the same time, increasing well-depth of the potential energy curve, that is, an increase in the dissociation energy. Overall, the results reported here improve our understanding of the electronic structure and behavior of the LiN molecule and its ions by providing spectroscopic constants, which are determined for the first time.

ACKNOWLEDGMENTS

The authors acknowledge the financial support of the Republic of Cyprus through the Research and Innovation Foundation project ML-NANOCAT (CODEVELOP-GT/0322/0093). This research was also supported by the EMME-CARE project, which has received funding from the European Union's Horizon 2020 Research and Innovation Program under Grant Agreement No. 856612, as well as matching co-funding by the Government of the Republic of Cyprus. The authors thank the Milan High-Performance Computing Facility of The Cyprus Institute for its computational resources.

DATA AVAILABILITY STATEMENT

The data that support the findings of this study are available from the corresponding author upon reasonable request.

ORCID

Somnath Bhowmick https://orcid.org/0000-0001-7498-2463

REFERENCES

[1] C. E. Dykstra, P. K. Pearson, H. F. Schaefer, *J. Am. Chem. Soc.* **1975**, *97*, 2321.
[2] S. Matsika, A. Papakondylis, A. Mavridis, *Chem. Phys. Lett.* **1996**, *250*, 409.
[3] K. Ishii, T. Taketsugu, K. Yamashita, *J. Chem. Phys.* **2007**, *127*, 194307.
[4] A. I. Boldyrev, J. Simons, P. von Schleyer, *J. Phys. Chem.* **1993**, *24*, 6149.
[5] A. I. Boldyrev, J. Simons, *J. Chem. Phys.* **1993**, *99*, 8793.
[6] D. Tzeli, A. Papakondylis, A. Mavridis, *J. Mol. Struct. THEOCHEM* **1997**, *417*, 277.
[7] A. P. L. Batista, F. R. Ornellas, *Comput. Theor. Chem* **2013**, *1009*, 17.
[8] M. Yuan, W. Li, M. Chen, *Int. J. Quantum Chem.* **2017**, *117*, e25380.

[9] C.-L. Yang, X. Zhang, K.-L. Han, *J. Mol. Struct.: THEOCHEM* **2004**, *676*, 209.
[10] J. Liang, C. Yang, L. Wang, Q. Zhang, *Chin. Opt. Lett.* **2011**, *9*, 120201.
[11] Y. Zhang, J. Xu, H. Yang, J. Xu, *RSC Adv.* **2022**, *12*, 19751.
[12] D. E. Woon, *Chem. Phys. Lett.* **1995**, *244*, 45.
[13] D. J. Frohman, P. F. Bernath, J. S. Brooke, *J. Quant. Spectrosc. Radiat. Transf.* **2016**, *169*, 104.
[14] I. Garcia-Cuesta, L. de Serrano-Andres, A. S. Meras, I. Nebot-Gil, *Chem. Phys. Lett.* **1992**, *199*, 535.
[15] D. M. Bittner, P. F. Bernath, *Astrophys. J., Suppl. Ser.* **2018**, *235*, 8.
[16] T. M. Rvachov, H. Son, A. T. Sommer, S. Ebadi, J. J. Park, M. W. Zwierlein, W. Ketterle, A. O. Jamison, *Phys. Rev. Lett.* **2017**, *119*, 143001.
[17] S. Dutta, D. S. Elliott, Y. P. Chen, *Europhys. Lett.* **2014**, *104*, 63001.
[18] L. D. Augustovičová, J. L. Bohn, *Phys. Rev. A* **2020**, *102*, 33314.
[19] M. Lara, P. Jambrina, F. Aoiz, J.-M. Launay, *J. Chem. Phys.* **2015**, *143*, 204305.
[20] J. L. Margrave, P. Sthapitanonda, *J. Chem. Phys.* **1955**, *59*, 1231.
[21] R. Herm, D. Herschbach, *J. Chem. Phys.* **1970**, *52*, 5783.
[22] Y. G. Khait, V. Baranovskii, *J. Struct. Chem.* **1982**, *23*, 167.
[23] H. Lischka, D. Nachtigallová, A. J. A. Aquino, P. G. Szalay, F. Plasser, F. B. C. Machado, M. Barbatti, *Chem. Rev.* **2018**, *118*, 7293.
[24] T. Shiozaki, H.-J. Werner, *Mol. Phys.* **2013**, *111*, 607.
[25] P. J. Knowles, H.-J. Werner, *Chem. Phys. Lett.* **1988**, *145*, 514.
[26] H.-J. Werner, P. J. Knowles, *J. Chem. Phys.* **1988**, *89*, 5803.
[27] S. R. Langhoff, E. R. Davidson, *Int. J. Quantum Chem.* **1974**, *8*, 61.
[28] H. J. Werner, P. J. Knowles, G. Knizia, F. R. Manby, M. Schütz, *Wiley Interdiscip. Rev. Comput. Mol. Sci.* **2012**, *2*, 242.
[29] P. J. Knowles, H.-J. Werner, *Chem. Phys. Lett.* **1985**, *115*, 259.
[30] H.-J. Werner, P. J. Knowles, *J. Chem. Phys.* **1985**, *82*, 5053.
[31] J. W. Hovick, J. C. Poler, *Chem. Educ.* **2005**, *82*, 889.
[32] J. D. Bender, S. Doraiswamy, D. G. Truhlar, G. V. Candler, *J. Chem. Phys.* **2014**, *140*, 54302.
[33] G. A. Daniel et al., *J. Chem. Phys.* **2020**, *152*, 184108.
[34] A. Berning, M. Schweizer, H.-J. Werner, P. J. Knowles, P. Palmieri, *Mol. Phys.* **2000**, *98*, 1823.
[35] R. J. Le Roy, *J. Quant. Spectrosc. Radiat. Transf.* **2017**, *186*, 167.
[36] https://physics.nist.gov.
[37] J. C. Rienstra-Kiracofe, G. S. Tschumper, H. F. Schaefer, S. Nandi, G. B. Ellison, *Chem. Rev.* **2002**, *102*, 231.
[38] S. Bhowmick, D. Hagebaum-Reignier, G.-H. Jeung, *J. Chem. Phys.* **2016**, *145*, 34306.
[39] J. A. Pople, R. Krishnan, H. B. Schlegel, J. S. Binkley, *Int. J. Quantum Chem.* **1978**, *14*, 545.

SUPPORTING INFORMATION

Additional supporting information can be found online in the Supporting Information section at the end of this article.

How to cite this article: M. D. Mohammadi, R. Bhaskaran, H. Y. Abdullah, H. H. Abdallah, G. Biskos, S. Bhowmick, *Int. J. Quantum Chem.* **2023**, e27288. https://doi.org/10.1002/qua.27288